JOURNAL OF GEOPHYSICAL RESEARCH, VOL. 102, NO. C11, PAGES 24,953–24,964, NOVEMBER 15, 1997

Deep tracer and dynamical plumes in the tropical Pacific Ocean

Gregory C. Johnson
Pacific Marine Environmental Laboratory/NOAA, Seattle, Washington

Lynne D. Talley
Scripps Institution of Oceanography, University of California San Diego, La Jolla

Abstract. Anomalous middepth plumes in potential temperature-salinity, θ-*S*, and buoyancy frequency squared, N^2, originate east of the East Pacific Rise Crest and decay toward the west. Conductivity-temperature-depth (CTD) data from recent hydrographic sections at 15°S and 10°N are used together with meridional sections at 110°, 135°, and 151°W to map these structures. Warm salty plumes west of the rise crest have maxima centered at 2700 m, 10°S and 8°N, and are interrupted by a cold, fresh tongue centered at 2900 m, 2°S. The θ-*S* anomalies decay to half their peak strength 2800 km to the west of the rise crest, ±300 km in the meridional, and ±0.4 km in the vertical. Vertical N^2 minima occur within the plumes, regions of reduced vertical gradients in θ and *S*. These minima are underlain by maxima near the depth of the rise crest, about 3200 m. The N^2 plumes decay more rapidly to the west of the rise crest than do the θ-*S* plumes. The N^2 structure is consistent with a pair of stacked gyres in each hemisphere. There are at least three possible mechanisms consistent with some aspects of these features. First, a deep maximum in upwelling somewhere below 2700 m would result in equatorward and westward interior flow at 2700 m, advecting these plumes along with it. Second, rapid upwelling of warm, salty, unstratified water in the eastern basins could result in westward overflows over the rise crest. Third, upwelling and associated entrainment processes owing to hydrothermal venting could result in stacked counter-rotating gyres west of the rise crest.

1. Introduction

Large-scale middepth δ^3He maxima are visible in the Geochemical Ocean Sections Study (GEOSECS) Pacific data, collected during 1973 and 1974 [*Ostlund et al.*, 1987, Plates 10 and 11]. These data are sparse, but both the western and eastern Pacific sections hint at low-latitude maxima between 2000 and 3000 m depth on either side of the equator. The data from this global survey are intriguing but do not definitively characterize the features or demonstrate their origins. Data from a subsequent survey at 15°S reveal a δ^3He plume with the highest values near 2500 m, a few hundred meters above the East Pacific Rise Crest [*Lupton and Craig*, 1981]. These high values are characteristic of emissions from the mantle and clearly come from hydrothermal vents at the rise crest. Values tail off to the west in a pattern reminiscent of smoke from a chimney. The plume suggests westward flow at this depth. *Lupton and Craig* [1981] note a feature in the density field that they term the "ridge crest front." They interpret this "discontinuity" in vertical profiles of potential density as the result of one water mass overlying another. A westward drift of water from the eastern basins over the rise crest might cause this front, coincident with the depth of the maximum δ^3He plume. The northern δ^3He maximum has also been explored. Detailed meridional δ^3He sections along 135°W clearly show the presence of the northern plume, slightly weaker than the southern one, and interrupted near 2°S by low-δ^3He water [*Craig*, 1990a, b; *Lupton*, 1996]. Another meridional section near the rise crest shows maxima at 5.5° and 9.5°N [*Craig*, 1991]. A δ^3He section at 10°N shows this weaker middepth maximum extending westward over much of the Pacific, originating above the rise crest [*Jenkins*, 1992]. A recent compilation of δ^3He data reveals the plumes in each hemisphere [*Lupton*, 1995].

Anomalously high values of potential temperature, θ, on a potential isopycnal near 3000 m (about 400 m below the maximum in δ^3He) can be traced from the East Pacific Rise Crest to at least 170°W between 10° and 20°S and may be linked to venting along the rise crest [*Reid*, 1982]. This warm salty temperature-salinity (θ-*S*) plume may be advected by westward flow in the region [*Reid*, 1986]. A more recent map of θ on a potential isopycnal near 2600 m, around the depth of the δ^3He maxima, reveals a warm salty plume extending to the west of the rise crest at around 8°N, separated from the warm salty plume centered around 10°S by colder, fresher water that extends eastward at around 2°S [*Talley and Johnson*, 1994]. This isopycnal is shallower than that used earlier [*Reid*, 1982], closer to the cores of these plumes, and reveals the slightly weaker northern plume. In addition, this shallower isopycnal surface does not ground in the basins east of the rise crest. Properties on this surface in these eastern basins suggest that the warm salty plumes may have their origin in modified North Atlantic Deep Water, which spreads north in the eastern basins and flows west over the rise crest at low latitudes. This observation prompts the suggestion that these plumes and their analogues in the Atlantic may be advected passively in the general circulation [*Talley and Johnson*, 1994].

Paper number 97JC01913.
0148-0227/97/97JC-01913$09.00

It should be emphasized here that even if the θ-*S* plumes are the result of venting and not westward spreading of water properties from the eastern basins, their warm salty nature cannot be directly related to heat flux from the venting but is determined by entrainment of ambient water during vertical ascent of the plume from the vent. A comparative study of Pacific and Atlantic hydrothermal plumes demonstrates that in the Pacific, which has a destabilizing deep ambient salinity gradient (salinity increasing with depth), a warm salty θ-*S* anomaly results from hydrothermal venting, whereas in the Atlantic, which has a stabilizing deep salinity gradient, the θ-*S* anomaly is cold and fresh [*Speer and Rona*, 1989].

A simple model for a dynamically active δ^3He plume has also been advanced [*Stommel*, 1982]. The plumes, entraining water as they ascend from the East Pacific Rise Crest to their neutrally buoyant level, may effect a significant mass sink at the rise crest and a mass source at their neutrally buoyant level, a few hundred meters higher. The heating at the rise crest not only alters the θ-*S* relation but deforms the density field, inducing a hydrothermally driven circulation at middepth. Isopycnals are pinched at the rise crest by the mass sink and spread at the neutrally buoyant level of the plume by the corresponding mass source. Thus a stacked gyre system might be driven, with a weakly stratified anticyclonic circulation above a more stratified cyclonic one. The gyres extend to the west, damped out by vertical diffusion. Since their signal is propagated more rapidly by Rossby waves at lower latitudes, they extend farther west there. This latitudinal variation in speed could make vents distributed evenly by latitude along the rise crest look like a single low-latitude source. This model is often referred to as the β plume. A background flow driven by a general upwelling, prominent in most theories of the abyssal circulation [*Stommel and Arons*, 1960], has been added to a model of the β plume to account for observed property distributions in the South Pacific [*Speer*, 1989]. In a similar study, deep upwelling strength and distribution, topography, geothermal heating strength, and geothermal heating location have all been shown to be of possible importance in a hierarchy of models of the abyssal flow of the South Pacific [*Hautala and Riser*, 1989].

A set of inverse calculations using density and tracer data yields an anticyclonic circulation west of the East Pacific Rise Crest at the depth of the South Pacific δ^3He plume [*Hautala and Riser*, 1993]. This result is the strongest evidence to date of a hydrothermally driven abyssal circulation. Interestingly, no cyclonic circulation is found below the anticyclone. Similarly, the combination of hydrographic and tracer data with a primitive equation model results in a deep anticyclonic gyre with no cyclonic gyre below (L. Yuan et al., Deep Pacific Ocean circulation inferred from the HELIOS Expedition data using a PE model, submitted to the *Journal of Physical Oceanography*, 1997; hereinafter referred to as Yuan et al., submitted manuscript, 1997). One possible reason for this absence could be an anticyclonic tendency induced by a hypsometric effect [*Rhines and MacCready*, 1989]. This effect is due to the increase in cross-sectional area of the ocean with decreasing depth, which results in a decrease in upwelling velocity with decreasing depth, forcing an anticyclonic tendency in the planetary geostrophic balance below the rise crest. Another possible reason is bottom mixing and geothermal heating along the western flank of the rise, which would tend to drive a bottom-intensified equatorward flow there [*Thompson and Johnson*, 1996], working against the formation of a deep cyclone.

Here conductivity-temperature-depth (CTD) data from two zonal transpacific hydrographic sections and three meridional hydrographic sections are used to examine the water mass and density structure at middepths in the tropical Pacific Ocean. The two zonal sections run along the north and south θ-*S* anomalies, and the three meridional sections cut across them. As discussed in many of the studies reviewed above, anomalies from a reference θ-*S* curve reveal warm salty water seemingly related to the δ^3He plumes, and the plumes appear to be associated with stratification extrema, which suggest dynamical activity. The distinguishing feature of this study is the uniform presentation of N^2 and θ-*S* anomalies using a set of high-resolution hydrographic sections that span the region inhabited by the plumes. In addition, the consistency of the property distributions and various dynamical frameworks for the middepth circulation are discussed.

2. Data

The data used here are the CTD data from the Transport of Equatorial Waters (TEW) transpacific section at nominal latitude 15°S [*Mangum et al.*, 1991], the Equatorial Pacific Interocean Circulation (EPIC) transpacific section at nominal latitude 10°N [*Equatorial Pacific Interocean Circulation Voyageurs*, 1991], and the meridional World Ocean Circulation Experiment (WOCE) sections P18 [*McTaggart et al.*, 1996], P17 [*Tsuchiya and Talley*, 1996], and P16 at nominal longitudes 110°, 135°, and 151°W (Figure 1). Stations on these cruises were usually occupied to within 10 m of the bottom.

The signals at this depth are small and subject to aliasing by eddies, internal waves, and other time-dependent phenomena. However, the CTD data are stable and densely sampled. The fields presented are smoothed heavily in the vertical and horizontal. The 2-dbar values of θ, salinity (*S*), θ-*S* anomaly (defined in section 3), and the square of buoyancy frequency, $\hat{N}$, are first averaged into 50-m depth bins starting from the bottom up. These quantities are objectively mapped assuming a Gaussian covariance with a horizontal correlation length of 150 km, a vertical correlation length of 125 m, and an error-to-signal energy of 1/16. The derivative quantity N^2 is noisier, so production of reasonably smooth maps requires doubling the correlation lengths and quadrupling the error-to-signal energy.

The θ-*S* anomalies are very small. In order to compare features among the five sections the salinity at θ = 1.6°C (near the peak θ-*S* anomaly, which is the primary region of interest) is found for all the stations, then values for each section are convolved with a five-point Hanning filter to obtain low-pass filtered values. The filtered values are found at the six crossover points (Figure 1), and a salinity offset is found for each section to minimize the differences of these values at the crossover points in a least squares sense (Table 1). These small adjustments are ad hoc. However, they do reduce differences at crossover points from as much as 0.0055 to <0.001 on the unitless 1978 practical salinity scale (pss-78). The adjustments are only applied to the θ-*S* anomalies since they are contoured at 0.001 intervals.

3. The θ-*S* Anomaly Plumes

Above the western flank of the East Pacific Rise in the tropics a deviation from a reference θ-*S* curve toward warm salty values is often present, with a maximum near θ = 1.6°C. This deviation increases toward the rise crest and peaks about ±10° from the equator. This pattern has been mapped previously in the horizontal by contouring θ on potential isopycnals [*Reid*, 1982; *Hautala and Riser*, 1993; *Talley and Johnson*, 1994]. To present

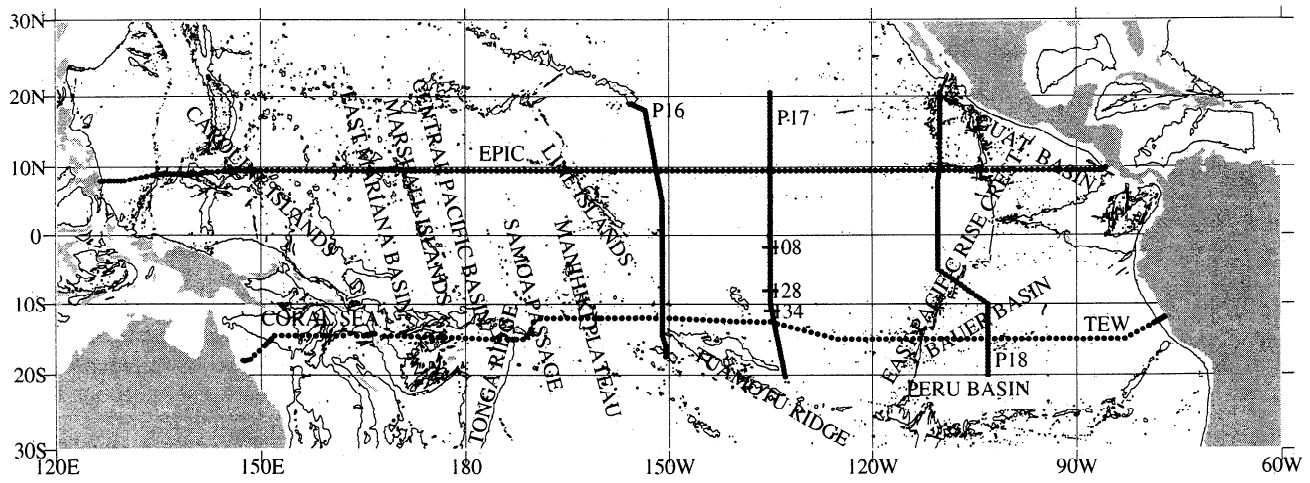

Figure 1. Station locations for the hydrographic data used in this study with the 3000 m isobath [*British Oceanographic Data Centre,* 1994]. Transport of Equatorial Waters (TEW) data [*Mangum et al.*, 1991] are at a nominal latitude of 15°S and Equatorial Pacific Interocean Circulation (EPIC) data [*Equatorial Pacific Interocean Circulation Voyageurs*, 1991] at 10°N. World Ocean Circulation Experiment (WOCE) section P18 data [*McTaggart et al.*, 1996] are at a nominal longitude of 110°W, WOCE section P17 data [*Tsuchiya and Talley*, 1996] are at 135°W, and WOCE P16 data are at 151°W.

vertical sections of this structure, we calculate a θ-*S* anomaly as a deviation from a reference θ-*S* curve constructed from a linear fit to the 50-dbar average θ-*S* data along 110°, 135°, and 151°W extending from 5°S to 5°N for θ < 3°C (Figure 2). Using a linear fit to the equatorial θ-*S* data is arbitrary, but the goal is to keep the reference curve as simple as possible to reveal the anomalies with a minimum of manipulation and allow discussion of them in a global sense. The slope of this reference θ-*S* curve is such that water that is 0.001 saline on an isotherm is 0.02°C warm on an isohaline. The same ratio holds for cold and fresh θ-*S* anomalies. Here θ-*S* anomalies will be presented in terms of salinity along isotherms. The θ-*S* anomalies calculated on appropriately referenced potential isopycnal surfaces would be similar in structure but reduced in magnitude by a factor of 2 from those calculated here.

At 15°S a plume of high θ-*S* anomaly decays and deepens westward from the East Pacific Rise Crest with a vertical maximum of 0.012 near 2550 m at 113°W to east of the Manihiki Plateau and a weaker vertical maximum near 2950 m at 164°W (Plate 1). The plume fades to half its strength around 2500 km to the west of the rise crest. While this feature is most germane to this discussion, a few other relevant features are described. The θ-*S* anomaly is high at the western and eastern ends of the sections, owing to the spreading of Lower Circumpolar Water from the south with a salty North Atlantic Deep Water influence into the Coral Sea (west of about 167°E) and the eastern deep basins (east of the rise crest at about 113°W). Warm salty Lower Circumpolar Water (at around 170°W, 3800

Table 1. Values Added to θ-*S* Anomalies So Differences Among the Deep θ-S Curves Are Minimized in a Least Squares Sense at Crossover Points

Nominal Section Location	θ-*S* Anomaly Adjustment, pss-78
151°W	−0.0015
135°W	0.0000
110°W	0.0015
10°N	−0.0010
15°S	−0.0030

Here θ-*S* is temperature-salinity; pss-78 is the unitless 1978 Practical Salinity Scale.

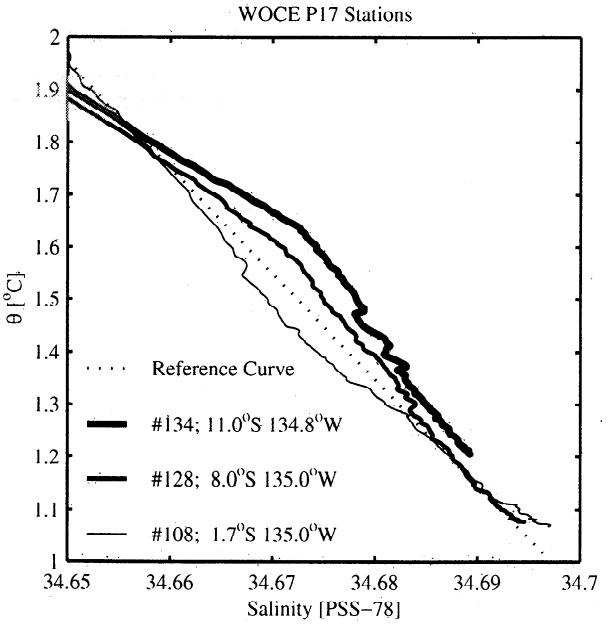

Figure 2. Reference temperature-salinity (θ-*S*) curve calculated from a linear fit to all the θ-*S* data from stations between 5°S and 5°N from WOCE sections P16, P17, and P18 along nominal longitudes 151°, 135°, and 110°W (dotted line). Also plotted are θ-*S* curves from P17 along 135°W at 11°S in the southern warm salty plume (thick solid line), at 8°S in a weaker part of the plume (intermediate solid line), and at 1.7°S in the cold fresh jet (thin solid line). The curves are only shown below 2°C to focus on the plume signature, evident as deviations from the reference curve between 1.3° and 1.8°C.

m) is also advected northward in the deep western-boundary current on its way toward the Samoa Passage. Just below this feature is Lower Circumpolar Water with a fresh cold Antarctic Bottom Water influence, also within the northward flowing deep western-boundary current. The boundary current is large, carrying about 12×10^6 m^3 s^{-1} of deep water that ventilates the deep Pacific to the north [*Taft et al.*, 1991; *Johnson et al.*, 1994; *Roemmich et al.*, 1996]. Above 2000 m the water is fresh because of the influence of Antarctic Intermediate Water from the south.

At 10°N, even more clearly than in the 15°S section, a middepth plume with a maximum exceeding 0.003 centered near 2600 m depth appears to originate from east of the East Pacific Rise, get boosted a bit at the crest (103°W), and then decay westward, almost like smoke from a chimney (Plate 2). The plume at the core depth decays to half strength about 2800 m from the rise crest, a distance very similar to that at 15°S. Other features of interest include the remaining salty North Atlantic Deep Water influence, which is seen near the bottom of the Central Pacific Basin (around 180°) and the East Mariana Basin (around 160°E). This influence is associated with Lower Circumpolar Water flowing northward in deep western-boundary currents in these two basins [*Johnson and Toole*, 1993]. Again, the fresh influence from above is due to the influence of Antarctic Intermediate Water since the warmer salinity minimum defining the North Pacific Intermediate Water does not extend south of 16°N in the Pacific Ocean interior [*Talley*, 1993]. As in the 15°S section, there are higher salinities to the east of the rise crest (around 103°W).

In the meridional sections (Plate 3) the maxima of the warm salty θ-S anomaly plumes are on average centered at 10°S, 2800 m, and 8°N, 2700 m. As in the zonal sections, the southern warm salty plume is over twice the strength of the northern one. Also as in the zonal sections, the warm salty plumes decay in strength to the west of the East Pacific Rise Crest. Estimates of the zonal decay to half strength of the maxima are about 2700 km to the west of the rise crest in both hemispheres, around one fifteenth of the way around the Earth. The meridional decay to half strength averages 300 ± 100 km, and the vertical decay to half strength averages 0.4 ± 0.1 km. Hence the zonal:meridional aspect ratio of these plumes is about 9:1. The meridional:vertical aspect ratio is about 750:1, so the zonal:vertical aspect ratio is about 6750:1. Another feature of some interest in the upper part of the meridional sections is the cold fresh influence of Antarctic Intermediate Water, which strengthens to the south, and a similar influence of North Pacific Intermediate Water, which strengthens to the north. The upper part of the sections is warmest and saltiest at around 2°–6°N, reflecting the fact that in the intermediate waters, only a weak Antarctic influence actually crosses the equator into the northern hemisphere while North Pacific influence does not extend far south of the northern subtropics.

Also of interest are some near-equatorial θ-S anomalies, one of which is negative near 1.5°S, 2900 m, at all three longitudes (Plate 3). This tongue is coldest and freshest at 151°W, decaying eastward to 110°W. It can be seen on an isopycnal map made somewhat above its core [*Talley and Johnson*, 1994]. Since this tongue actually deviates on the cold and fresh side of a linear curve, it is not likely that vertical processes alone are causing this minimum between the two positive plumes. It is much more likely that the tongue is a result of advection of cold, fresh water from the west near the equator. Direct velocity measurements taken during the meridional WOCE sections support this assertion (E. Firing et al., Equatorial subthermocline currents across the Pacific, submitted to the *Journal of Geophysical Research*, 1996; hereinafter referred to as Firing et al., submitted manuscript, 1996). In addition, direct velocity measurements taken along 159°W from March 1982 to June 1983 show a robust eastward jet centered at 1.5°S, 3100 m [*Firing*, 1989], with an estimated transport of 6–7 $\times$ 10^6 m^3 s^{-1}. This eastward advection of cold, fresh, low-δ^3He water may help to separate the northern and southern plumes [*Craig* 1990a, b]. Higher up in the water column, there is a warm salty tongue at 1.5°S, 2000 m that weakens from east to west, suggesting that a westward jet near this depth may be carrying water in the opposite direction of the cold fresh tongue that weakens from west to east about 900 m below. This tongue has not been previously described and may be linked to the westward current centered about 1.5°S, 1800 m, which is visible but has not been described at 159°W and in the WOCE velocity measurements [*Firing*, 1989; Firing et al., submitted manuscript, 1996].

The 110°W section crosses the East Pacific Rise Crest near 7°S (Figure 1 and Plate 3). The water near 2800 m here is warm and salty, with anomalies exceeding 0.006. Here the section samples the southern warm salty plume to the north of its maximum values, so it is weaker and farther north than the southern plume in the meridional section at 135°W. The northern θ-S anomaly maximum near 2700 m is broad and exceeds 0.003 from nearly 2° to 10°N. The cold fresh tongue at 1.5°S, 2900 m is relatively weak compared to the meridional sections to the west, whereas the warm salty tongue at 2°S, 2000 m is very strong. Also of interest, the deep water in the 110°W section is relatively warm and salty in the Peru Basin, south of 16.5°S, reflecting a North Atlantic Deep Water influence coming directly from the south, east of the rise crest. However, in the Bauer Basin, between 16.5° and 7°S, water of $\theta < 1.5$°C is relatively fresh, supporting results from previous studies suggesting that it comes from the Central Pacific Basin over the rise crest [*Lonsdale*, 1976]. Higher in the water column, near 2800 m, a wedge of salty water from the south can be seen intruding north of 16.5°S.

At 135°W the maximum of the southern warm salty plume is located near 11.5°S, 2700 m exceeding 0.008 (Plate 3). It is stronger and a few degrees farther south than at 110°W, supporting the suggestion that the 110°W section crosses the East Pacific Rise Crest too far north to sample the entire plume. The northern warm salty plume, with a small maximum exceeding 0.002 near 8°N, 2750 m, has weakened and narrowed. The cold fresh tongue at 1.5°S, 2800 m, and the warm salty tongue at 2°S, 2000 m, are both of intermediate strength compared to the sections to the east and west.

By 151°W both the southern and northern warm salty plumes have weakened considerably and moved equatorward by 1°–2° latitude (Plate 3). The southern plume maximum exceeding 0.005 is located at 8.5°S, 2950 m, and the northern maximum over 0.001 is located at 6°N, 2850 m. As in all the sections, the southern plume is stronger than the northern. The cold fresh tongue at 1.5°S, 2950 m, is strongest at 151°W, and the warm salty tongue at 2°S, 2050 m, is weakest at 151°W. Their monotonic zonal trends in the meridional sections support advection to the east near 2900 m and advection to the west near 2000 m, as seen at 159°W [*Firing*, 1989].

4. Buoyancy Frequency Plumes

The buoyancy frequency squared, $N^2 = -g/\rho \, \partial\rho/\partial z$, is proportional to the strength of the vertical density stratification, where ρ is the potential density referenced to the central

pressure of the range over which the vertical gradient is estimated and g is the gravitational acceleration. If relative vorticity is much smaller than the local Coriolis parameter, $f = 2\Omega\sin\phi$, the vertical component of potential vorticity can be approximated by $Q \approx f/gN^2$. Here Ω is the rotation rate of the Earth, and ϕ is the latitude. This approximation is probably reasonable in the deep interior ocean except within a few degrees of the equator. This dynamical tracer, Q, is conserved along streamlines in nondiffusive, geostrophic flow. Vertical sections of N^2 complement the θ-S anomaly sections, adding dynamical insight because of their relation to density and potential vorticity. In the oceans, N^2 decreases markedly below the pycnocline, falling to very low values in the deep and bottom waters. Below 2500 m in the interior of the tropical Pacific Ocean, values tend to fall between 0.6×10^{-6} s^{-2} and 0.8×10^{-6} s^{-2}. The exceptions from these background values are described below. As before, the zonal sections are described first, followed by the meridional sections from east to west.

At 15°S (Plate 1), unlike at 10°N (Plate 2), there is no obvious plume signature in N^2 west of the East Pacific Rise Crest. However, there are several interesting departures from background N^2 values below 2500 m along 15°S worthy of description. First, there is a large area of reduced N^2 east of the rise crest at 112°W in the deep Bauer and Peru Basins. This low stratification could be due to a combination of at least three factors: diffusion near the bottom boundary, geothermal conductive heating at the bottom, and the basins being filled with nearly homogeneous water by a dense overflow at a shallow sill or sills in the ridges that define them. It will be suggested in section 5 that this water may supply at least some part of the N^2 plume minima discussed in the remaining sections. Second, in the bottom several hundred meters the stratification decreases drastically towards the bottom. Along gentle slopes such as the western flank of the rise (160°–112°W), the isotherms also slope down toward the topography, suggesting a bottom-intensified, equatorward flow in the region. These phenomena have been modeled as the combined effects of diffusion and geothermal heating at the bottom boundary [*Thompson and Johnson*, 1996]. Third, there is a local vertical maximum in stratification at the western edge of the Central Pacific Basin that reaches 3650 m against the Tonga Ridge (175°W) and falls to near 4300 m by the Manihiki Plateau (165°W). This structure is located at the top of the warm salty modified North Atlantic Deep Water, part of the northward flowing deep western-boundary current [*Johnson et al.*, 1994].

The 10°N section sports a plume of low N^2 extending westward from the East Pacific Rise Crest near 103°W, 2500 m, to nearly 150°W and a region of elevated N^2 just below it at about 3000 m (Plate 2). The N^2 minimum and maximum below are associated with the warm salty plume centered at 8°N, 2700 m. Such an N^2 doublet is weak or nonexistent in the 15°S section, probably because it is too far south to cut through a weaker but analogous structure in the southern hemisphere. Also of interest is the large area of low stratification in the deep Guatemala Basin east of the rise crest at 103°W. The warm, salty, reduced stratification plume water west of the rise crest may have at least a partial source in the Guatemala Basin. Again, there is reduced stratification some distance above the rise flank with isotherms plunging toward the bottom. However, the stratification is no longer high where the two branches of the deep western-boundary current bank against the Caroline (150°E) and Marshall (175°E) Islands [*Johnson and Toole*, 1993], probably because the potential vorticity in that current is reset to near zero by frictional processes where it crosses the equator.

In the 110°W section there is a strong plume of low stratification near 2750 m, extending north (and west) of the rise crest at 6.5°S (Plate 3). Just below and to the northwest of this minimum is a relative maximum. From 2° to 9°N a similar N^2 doublet exists, with a minimum near 2650 m and a maximum near 3150 m. Both north and south of the equator, the N^2 minimum is associated with the warm salty plume, and the N^2 maximum lies several hundred meters below it. This section again shows low stratification in the basins east of the East Pacific Rise Crest (20°–7°S) and within several hundred meters of the bottom over gentle slope. In addition, there is smaller vertical wavelength structure apparent in N^2 within a few degrees of the equator, with three minima and two maxima below 2500 m.

At 135°W, west of the East Pacific Rise Crest in both hemispheres, the N^2 doublet south of the equator is weaker than that north of the equator (Plate 3). In the south the minimum is strongest near 2650 m between 7° and 13°S while the maximum, around 3050 m, is offset equatorward from the minimum at 3°–10°S. These structures are broad, with no localized maximum in the horizontal. In the north the minimum is centered at 2600 m from 2° to 9°N, and the maximum lies below it near 3050 m. The northern extrema are clearly strongest near 3.5°N. On both sides of the equator the doublets are weaker compared to those to the east and stronger than those to the west. Again, smaller vertical wavelength structure is evident near the equator.

By 151°W the southern hemisphere signal is weak or nonexistent (Plate 3), with a hint of a minimum from 9° to 13°S at 2950 m and a very weak maximum centered at 10.5°S, 3450 m. The northern hemisphere doublet is clearer, with a minimum near 2650 m, and a maximum near 3150 m. Both extrema extend from 2° to 6°N, and are most extreme near 3°N. The smaller vertical wavelength structure near the equator persists in the same pattern as at 110° and 135°W.

These paired vertical extrema in both hemispheres, strongest near the East Pacific Rise Crest and decaying to the west, suggest that stacked gyres of opposite sign circulation may exist in the region on both sides of the equator. The top minima in N^2 near 2700 m on either side of the equator are consistent with an anticyclonic circulation (clockwise in the northern hemisphere). The bottom maxima are consistent with a cyclonic circulation, as predicted by the β plume theory [*Stommel*, 1982]. These deep N^2 maxima are the first observational suggestions of the existence of these gyres, searched for but not found in the sparser grid of the Helios expedition hydrographic data [*Hautala and Riser*, 1993; Yuan et al., submitted manuscript, 1997].

What are the relative strengths of these gyres? The thermal wind equation, $f\partial u/\partial z = g/\rho\ \partial\rho/\partial y$, can be differentiated once in the vertical then combined with the definition of buoyancy frequency squared, $N^2 = -g/\rho\ \partial\rho/\partial z$, to obtain the equation $f\partial^2 u/\partial z^2 = -\partial N^2/\partial y$. Define the gyre center as y_0, one gyre edge as y_1, and the distance between them as L. The N^2 structure (see Plate 3) between y_0 and y_1 can be idealized as the product of a sinusoidal mean vertical structure with a vertical wavenumber λ and a horizontal structure that increases linearly from 0 at y_1 to an amplitude A at y_0, so that between y_1 and y_0, $\partial N^2/\partial y = A\sin\lambda z / L$. Substituting the latter expression into the former, then integrating once in the meridional from y_0 to y_1 and three times in depth over half a wavelength, gives an expression for the zonal mass transport in each limb of these gyres, $M = 2A/f\lambda^3$.

For the northern gyres, $A = 5 \times 10^{-6}$ s^{-2} and $\lambda = \pi/500$ m seem

appropriate (Plate 3). Hence the equatorward limbs, between 1° and 3.5°N, have a strength of around 7×10^6 m^3 s^{-1}, with peak velocities near 0.08 m s^{-1}. The poleward limbs, between 3.5° and 11.5°N, have a strength closer to 2×10^6 m^3 s^{-1} with peak velocities near 0.008 m s^{-1}. The southern signals are weaker and not coincident in latitude, but $A = 3 \times 10^{-6}$ s^{-2} and $\lambda = \pi/500$ m seem appropriate (Plate 3). The equatorward limbs, between roughly 4° and 8°S, carry about 2×10^6 m^3 s^{-1} with peak velocities near 0.01 m s^{-1}. The poleward limbs, between roughly 8° and 13°S, carry about 1×10^6 m^3 s^{-1} with peak velocities near 0.005 m s^{-1}. The discrepancies in velocity and mass transport between the two limbs of the gyres in each hemisphere result from the rapid fractional change in Coriolis parameter with increasing distance from the equator at low latitudes. The circulation implies net westward transports of 5×10^6 m^3 s^{-1} and 1×10^6 m^3 s^{-1} in the northern and southern anticyclonic gyres, respectively. A similar asymmetry is implied for the cyclonic gyres, with net eastward transports. To close the circulation, net eastward transports in the lower gyres and net westward transports in the upper gyres imply a conversion of cold water to warm water at or east of the East Pacific Rise Crest. The ramifications of these conversions are discussed in detail below.

5. Discussion

Three dynamical frameworks are advanced in attempts to account for some of the patterns seen in the data. These models are presented from simplest to most involved and feature upwelling concentrated in the basins to the west of the East Pacific Rise Crest, in the basins to the east of the crest, and at the crest, respectively. Although none of the models explain all of the observations, their order of presentation also reflects increasing agreement with observational patterns.

The simplest dynamical framework is a two-layer elaboration of the classical one-layer dynamical framework for the deep circulation [*Stommel and Arons*, 1960]. In the one-layer framework, interior upwelling at the top of a deep layer drives an eastward and poleward interior flow through planetary geostrophy and a no-flux boundary condition at the eastern edge, separating the eastern and western basins for simplicity. Water to supply this interior upwelling comes east from deep western-boundary currents fed by localized sinking at high latitudes and recirculation of interior flow. This one-layer model is obviously at odds with the plumes of warm, salty, weakly stratified water originating at or east of the East Pacific Rise Crest and extending to the west on either side of the equator. However, if the interior upwelling were to increase in magnitude to the top of a bottom layer and then decrease to the top of a deep layer, the bottom layer would look like the one-layer case, but the deep layer would be reversed in direction and have a westward and equatorward interior flow and a deep western-boundary current carrying water back toward the high latitudes (Figures 3a and 3b). In each layer the interior flow is matched to a deep western-boundary current. This circulation scheme is in accord with observational evidence from geostrophic calculations using hydrographic section data, which suggest northward bottom flow offset by southward deep flow in the central basins of the South Pacific [*Warren*, 1973; *Wunsch et al.*, 1983; *Reid*, 1986] and the North Pacific [*Roemmich and McCallister*, 1989; *Bryden et al.*, 1991; *Johnson and Toole*, 1993]. If the level of the maximum upwelling were directly below the warm, salty, weakly stratified water, it would be carried westward by the interior flow, creating a plume as observed. However, this simple framework treats the ocean as two separate basins with similar but separate circulations. It does not account for the high stratification below the warm, salty, weakly stratified layer; the apparent vertically stacked gyres implied by the density field; nor for the apparent conversion of cold water into warm water at or east of the rise crest.

A second, more complicated model supposes that sources of bottom water feed upwelling in the deep basins east of the East Pacific Rise Crest (Figures 3c and 3d). The source could be a deep western-boundary current from the south [*Warren*, 1973] or a deep jet from the west [*Firing*, 1989] feeding through a fracture zone in the rise crest, as suggested by previous results [*Lonsdale*, 1976], and in section 3 by the cold fresh θ-S anomaly below $\theta = 1.6$°C along 103°W in the Bauer Basin (Plate 3). In the schematic both sources contribute equally to the upwelling: a lower-layer deep western-boundary current flowing northward in the eastern basin, and a strong eastward flow in the equatorial limb of the cyclonic circulation in the lower layer of the western basin, some of which crosses through a gap in the rise crest. Whatever the distribution of sources, this water fills these basins over sills, creating a nearly homogenous water mass that is further mixed and heated by diffusive and geothermal processes [*Lonsdale*, 1976; *Joyce et al.*, 1986; *Thompson and Johnson*, 1996]. As this water becomes lighter under these influences, it upwells to ride above the more recently arrived bottom inflow and eventually ascends to a depth where it breaks the topographic constraint imposed by the rise crest and flows westward along geostrophic characteristics into the Central Pacific Basin, strengthening the equatorial limb of the western basin anticyclone in the upper layer. These warm, salty, less-stratified overflows sliding into the water column of the Central Pacific Basin constitute a local N^2 minima and could increase the stratification above and below, strengthening the deep local N^2 maxima. However, the maximum θ-S anomaly above the rise crest is associated with the elevated δ^3He values outlined in the introduction. Hence, in this scenario, water from the eastern basins must gain at least some of these properties as they pass over the rise crest, but they would be passive tracers only.

The third, most complicated model is the β plume [*Stommel*, 1982]. In this model, geothermal plumes at the East Pacific Rise Crest effect a mass transfer from the depth of the crest to a plume equilibrium height a few hundred meters shallower (Figures 3e and 3f). This mass transfer drives an anticyclonic gyre at the plume equilibrium height over a cyclonic gyre at rise crest depth. The cold water from the strong eastward flow in the equatorward limb of the lower-layer cyclonic circulation is converted to strengthen the westward flow in the equatorial limb of the upper-layer anticyclonic circulation. The gyres are consistent with the observed stratification extrema. The anticyclonic gyres are revealed by the shallower stratification minima, where fluid is added by the plumes, and the cyclonic gyres are revealed by the deeper stratification maxima, where fluid is withdrawn. The observations here of the deeper stratification maxima, especially strong in the northern hemisphere, are the first evidence of the cyclonic gyres predicted by this theory. The conversion from colder to warmer water is also accounted for by the plume entrainment process. One possible discrepancy is that the θ-S plumes in the meridional sections show maximum values poleward of the westward limbs of the upper gyres (which are on the equatorward side of the stratification minima), not along the westward limbs as predicted by the β plume model [*Stommel*, 1982].

Both the N^2 minima and the warm salty θ-S plumes are

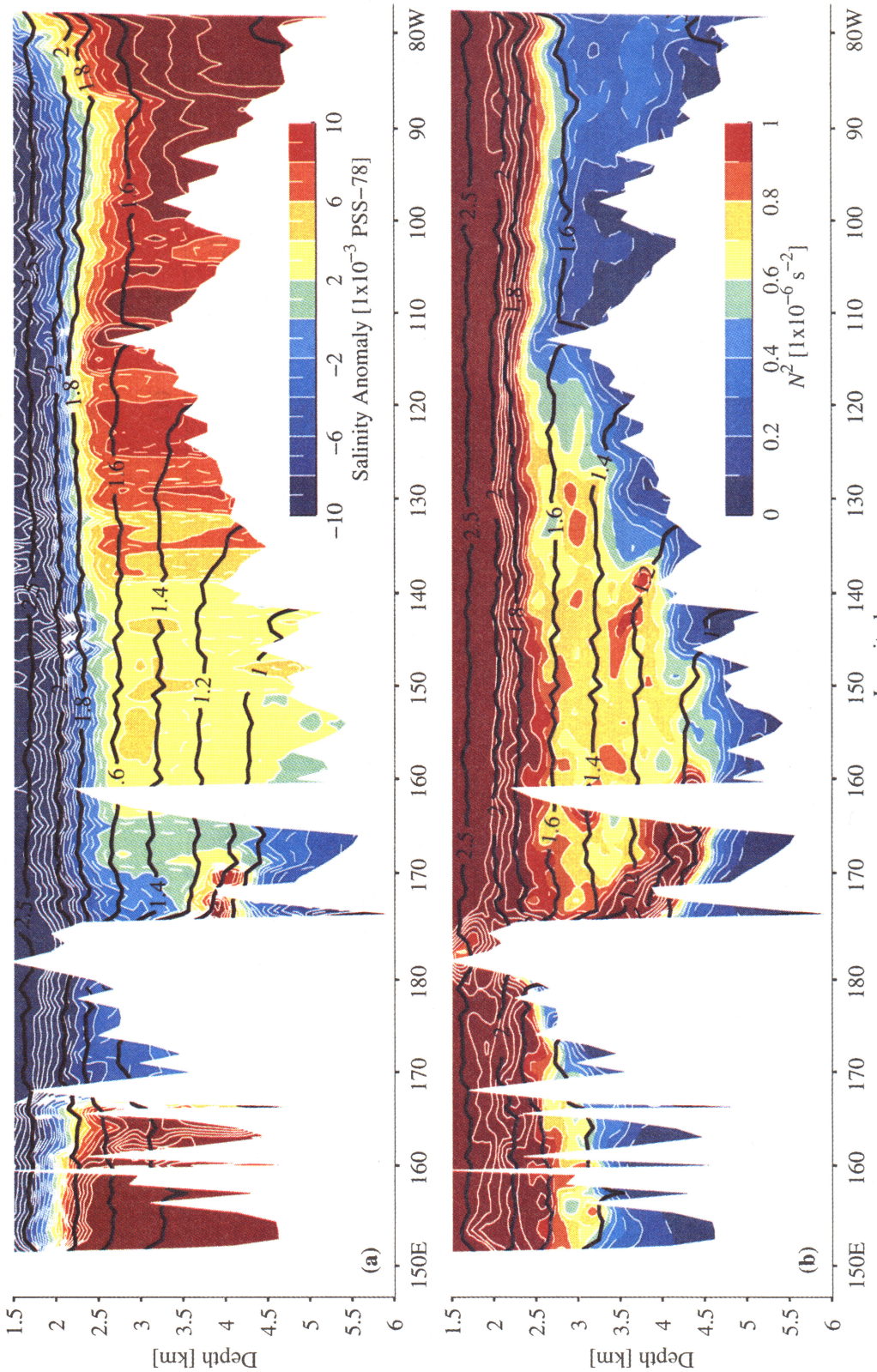

Plate 1. (a) A vertical section of θ-*S* anomaly and (b) a vertical section of buoyancy frequency squared, N^2, at 15°S. Vertical exaggeration is 1000:1 with longitudes plotted on the horizontal axis. On both sections potential isotherms are contoured every 0.2°C to 2.0°C and every 0.5°C in warmer water (thick black labeled lines). Fields are objectively mapped as described in the text. The θ-*S* anomaly (Plate 1a) is contoured at 0.002 (pss-78) from –0.020 to 0.020 (solid white lines) and –0.009 to 0.009 (dashed white lines) and shaded over a range of –0.010 to 0.010 at 0.002 intervals (color bar). The θ-*S* anomaly is calculated as a salinity deviation from the θ-*S* reference curve (Figure 2) at constant potential temperature with offset applied by section (Table 1). N^2 (Plate 1b) is contoured at 2×10^{-6} s^{-2} intervals from 0 to 20×10^{-6} s^{-2} (solid white lines) and from 1×10^{-6} s^{-2} to 9×10^{-6} s^{-2} (dashed white lines) and shaded over a range of 0 to 10×10^{-6} s^{-2} at 1×10^{-6} s^{-2} intervals (color bar).

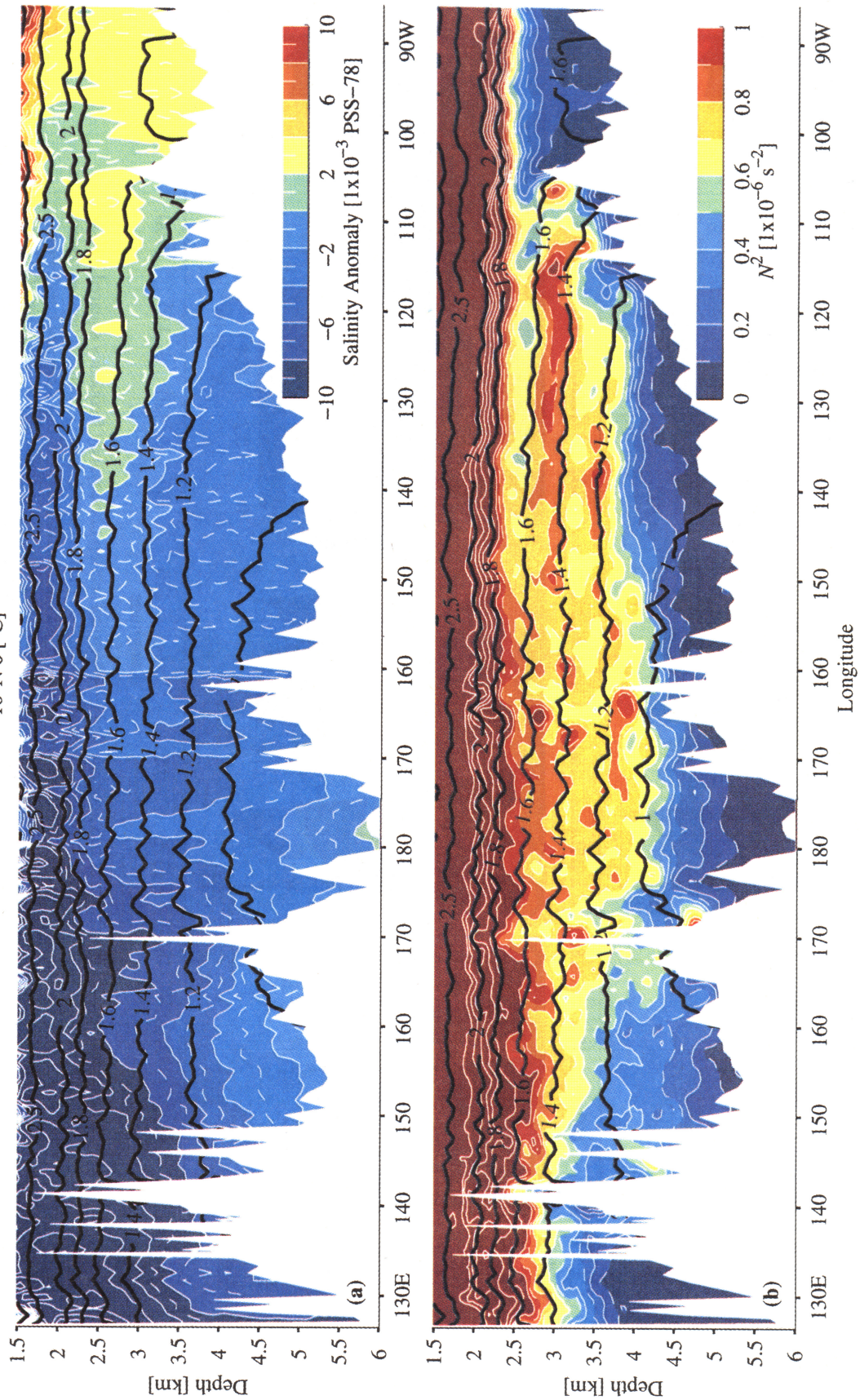

Plate 2. (a) A vertical section of θ-*S* anomaly and (b) a vertical section of buoyancy frequency squared, N^2, at 10°N. Details as in Plate 1.

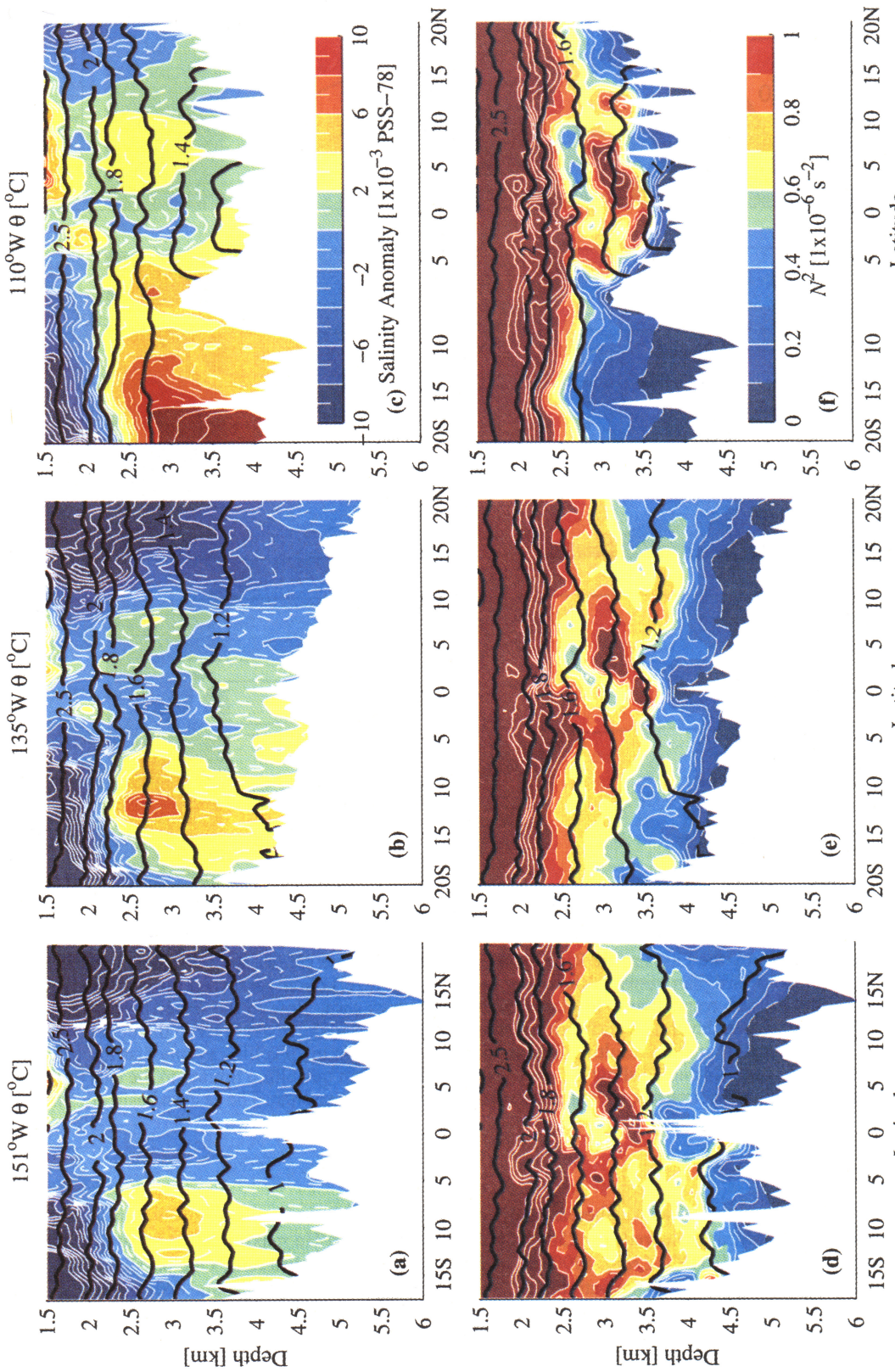

Plate 3. (a–c) Vertical sections of θ-*S* anomaly and (d–f) vertical sections of buoyancy frequency squared, N^2, at 151°, 135°, and 110°W (left to right). Details as in Plate 1 except latitudes are plotted on the horizontal axis.

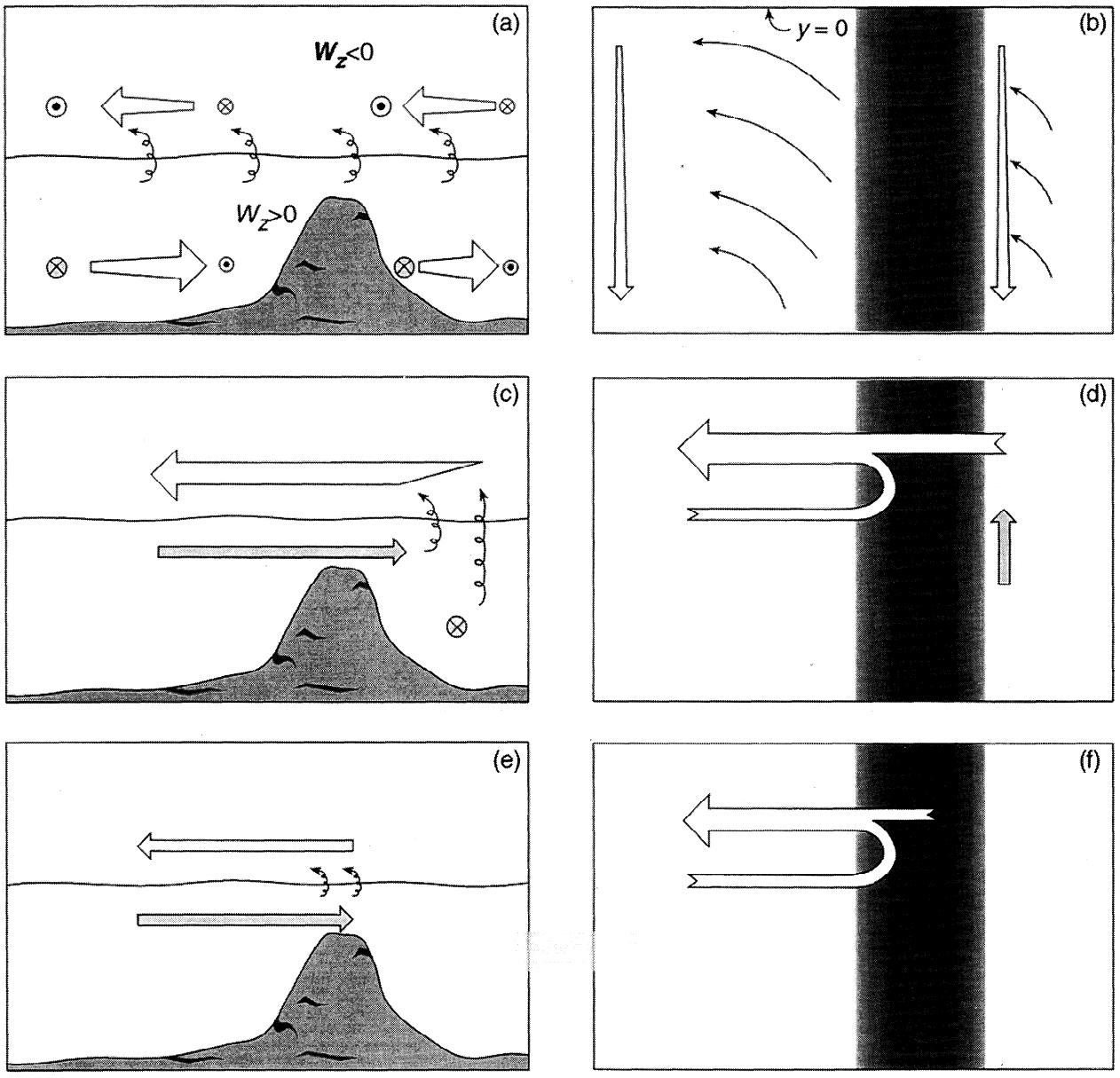

Figure 3. Schematic two-layered southern hemisphere circulations for the three different upwelling scenarios with two basins separated by the East Pacific Rise. Figures 3a, 3c, and 3e are side views of the net circulation, and Figures 3b, 3d, and 3f are plan views of the upper layer (plume-level) circulation with the rise crest and flanks shaded dark and light, respectively, in plan view. Open arrows show flow in the upper layer, shaded arrows show flow in the lower layer, and curly arrows show upwelling from the lower layer to the upper layer. Figures 3a and 3b show the circulation resulting from a middepth maximum in upwelling evenly distributed on both sides of the rise. Figures 3c and 3d show the circulation resulting from upwelling limited to the east of the rise. Figures 3e and 3f show the circulation resulting from upwelling at the rise crest. The eastern basin does not play a role in this last scenario.

located around 2700 m and deepen to the west, whereas the δ^3He plumes described in the literature are centered near 2500 m [*Lupton and Craig*, 1981; *Ostlund et al.*, 1987; *Craig*, 1990a, b, 1991; *Jenkins*, 1992; *Lupton*, 1995; 1996]. If the low-stratification, warm salty water simply slides westward over the East Pacific Rise Crest from the eastern basins and sweeps along vented fluid on the way, then the 200 m depth difference is not particularly problematic. In fact, one might reasonably expect the vented δ^3He to rise through the N^2 minima until it is stopped by the stronger stratification above, making for a natural vertical displacement of these features. However, if the θ-S anomalies, N^2 minima, and δ^3He maxima all originate from the venting, why are their depths different? One possible answer lies in the vertical profiles of the background distributions and the effects of vertical mixing. The source of the δ^3He maximum is the vent plumes, which reach an equilibrium height near 2500 m. The background distribution of δ^3He is minimal, so the property has a roughly Gaussian shape centered around 2500 m in the vertical, probably a result of the effects of vertical mixing. Plotting θ and S against depth reveals that the θ-S anomalies are

associated with reduced vertical gradients in θ, *S*, and (of course, since N^2 is a minimum) ρ centered near 2700 m, tending deeper to the west. The deep background gradients of θ, *S*, and ρ are all low near the bottom and increase upward in a roughly exponential manner. This background distribution tends to increase curvature of these properties at the top of the plume regions and reduce curvature at the base of these regions. Hence vertical mixing can more effectively erode the top of the reduced gradients than the base, causing the signatures to deepen with time (hence distance) from the source.

One significant result of this analysis that is unexplained by any of these frameworks is that the southern hemisphere θ-*S* anomaly (the passive tracer) is stronger, but the northern hemisphere N^2 extrema (the dynamically active tracer) are stronger. The relative strength of the southern hemisphere θ-*S* anomaly could be due to its relative proximity to the warm salty modified North Atlantic Deep Water in the eastern basins, which spreads from the south [*Reid*, 1986; *Talley and Johnson*, 1994]. The relative strength of the northern N^2 extrema might come from the fact that the East Pacific Rise in the northern hemisphere is isolated from the southern sources of deep water, which must cross the equator at a western boundary because of the strong potential vorticity constraint [*Stommel and Arons*, 1960; *Kawase*, 1987]. The resulting quieter background stratification in the northern hemisphere would allow the gyres obeying the second or third frameworks to establish more strongly there. In addition, currents around the nearby Tuamotu Ridge in the southern hemisphere may also make the deep circulation there more complex, working to prevent the establishment of a simple gyre signature associated with the stratification.

Finally, in both gyres the equatorward limbs transport more water than the poleward limbs, which means that cold water is brought in from the west in the deeper cyclonic gyres and warmer water is returned to the west in the shallower cyclonic gyres. While a precise calculation of the magnitude of the effect is difficult, estimates are of order $1–5 \times 10^6$ m^3 s^{-1}. The deeper flow from the west could also be supplied by the eastward jet carrying 6×10^6 m^3 s^{-1} between 3°S and 1°N at a depth near 3100 m, observed directly at 159°W [*Firing*, 1989], consonant with the cold fresh tongue seen in all three meridional sections near 1°–2°S, 2900 m. An eastward flow at this depth was posited to supply bottom water from the Central Pacific Basin to the Guatemala and Bauer Basins through a gap in the East Pacific Rise Crest at 3°S [*Lonsdale*, 1976]. The depth and temperature differences between the stratification extrema are about 500 m and 0.2°C, which for an upwelling of 3×10^6 m^3 s^{-1} in each hemisphere implies a heating of 2.4×10^{12} W. Convective heating along the rise crests [*Lupton*, 1995] is about a third of the magnitude implied here. Additional sources for the implied conversion might be conductive heating through the floors of the eastern basins [*Lonsdale*, 1976] or, simply, downward diffusion of heat by topographically induced mixing in the region.

Acknowledgments. GCJ is funded by the Climate and Global Change Program through the NOAA Office of Global Programs. LDT is funded through NSF Ocean Sciences grants OCE89-18961 and OCE90-04394. The chief scientists for the cruises from which hydrographic data were used were Stan Hayes and David Behringer for TEW; John Toole and Harry Bryden for EPIC; Lynne Talley and Gregory Johnson for WOCE P16C; Lynne Talley, Mizuki Tsuchiya, and James Swift for WOCE P17C; and Gregory Johnson and Bruce Taft for WOCE P18. Conversations with Kevin Speer, Bruce Warren, Terry Joyce, LuAnne Thompson, and Susan Hautala were stimulating. The two anonymous reviewers made comments that improved the manuscript. PMEL contribution number 1790.

References

British Oceanographic Data Centre (BODC), *Supporting volume to the GEBCO Digital Atlas*, Br. Oceanogr. Data Cent., Birkenhead, England, 1994.

Bryden, H. L., D. H. Roemmich, and J. A. Church, Ocean heat transport across 24°N in the Pacific, *Deep Sea Res., Part A, 38*, 297–324, 1991.

Craig, H., The HELIOS Helium 3 section: Implications for the deep water circulation in the North and South Pacific (abstract), *Eos Trans. AGU, 71*, 882, 1990a.

Craig, H., The HELIOS Helium 3 Jets in the North and South Pacific (abstract), *Eos Trans. AGU, 71*, 1396, 1990b.

Craig, H., Hydrothermal plumes at 5 & 9 degrees north on the EPR and the origin of the northern hemisphere zonal helium jet (abstract), *Eos Trans. AGU, 72*(44), Fall Meet. Suppl., 491, 1991.

Equatorial Pacific Interocean Circulation (EPIC) Voyageurs, Hydrographic data from the 10°N transpacific cruise R/V *Moana Wave* cruise #89-3, -4, -6, *Tech. Rep. WHOI-91-32*, 287 pp., Woods Hole Oceanogr. Inst., Woods Hole, Mass., 1991.

Firing, E., Mean zonal currents below 1500 m near the equator, 159°W, *J. Geophys. Res., 94*, 2023–2028, 1989.

Hautala, S. L., and S. C. Riser, A simple model of abyssal circulation, including effects of wind, buoyancy, and topography, *J. Phys. Oceanogr., 19*, 596–611, 1989.

Hautala, S. L., and S. C. Riser, A nonconservative β-spiral determination of the deep circulation in the eastern South Pacific, *J. Phys. Oceanogr., 23*, 1975–2000, 1993.

Jenkins, W. J., Tracers in oceanography, *Oceanus, 35*, 47–56, 1992.

Johnson, G. C., and J. M. Toole, Flow of deep and bottom waters in the Pacific at 10°N, *Deep Sea Res., Part I, 40*, 371–393, 1993.

Johnson, G. C., D. L. Rudnick, and B. A. Taft, Bottom water variability in the Samoa Passage, *J. Mar. Res., 52*, 177–196, 1994.

Joyce, T. M., B. A. Warren, and L. D. Talley, The geothermal heating of the abyssal subarctic Pacific Ocean, *Deep Sea Res., Part A, 33*, 1003–1015, 1986.

Kawase, M., Establishment of deep ocean circulation driven by deep-water formation, *J. Phys. Oceanogr., 17*, 2294–2317, 1987.

Lonsdale, P., Abyssal circulation of the southeastern Pacific and some geological implications, *J. Geophys. Res., 81*, 1163–1172, 1976.

Lupton, J. E., Hydrothermal plumes: Near and far field, in *Seafloor Hydrothermal Systems: Physical, Chemical, Biological, and Geological Interactions*, *Geophys. Monogr. Ser.*, vol. 91, edited by S. E. Humphris et al., pp. 317–346, AGU, Washington, D. C., 1995.

Lupton, J. E., A far-field hydrothermal plume from Loihi Seamount, *Science, 272*, 976–979, 1996.

Lupton, J. E., and H. Craig, A major helium-3 source at 15 °S on the East Pacific Rise, *Science, 214*, 13–18, 1981.

Mangum, L., J. Lynch, K. McTaggart, L. Stratton, and S. Hayes, CTD/O_2 data measurements collected on TEW (Transport of Equatorial Waters) June–August 1987, *NOAA Data Rep. ERL PMEL-51*, 375 pp., Pac. Mar. Environ. Lab., Seattle, Wash., 1991.

McTaggart, K. E., G. C. Johnson, and B. A. Taft, CTD/O_2 measurements collected on a climate and global change cruise (WOCE Section P18) along 110°W during January-April, 1994,

NOAA Data Rep. ERL PMEL-59, 519 pp., Pac. Mar. Environ. Lab., Seattle, Wash., 1996.

Ostlund, H. G., H. Craig, W. S. Broecker, and D. Spencer, *GEOSECS Atlantic, Pacific, and Indian Ocean Expeditions*, Vol. 7, *Shorebased Data and Graphics*, 200 pp., Natl. Sci. Found., Washington, D. C., 1987.

Reid, J. L., Evidence of an effect of heat flux from the East Pacific Rise upon the characteristics of middepth waters, *Geophys. Res. Lett., 9*, 381–384, 1982.

Reid, J. L., On the total geostrophic circulation of the South Pacific Ocean: Flow patterns, tracers and transports, *Prog. Oceanogr., 16*, 1–61, 1986.

Rhines, P. B., and P. MacCready, Boundary control over the large-scale circulation, in *Proceedings of the Fifth 'Aha Huliko'a Hawaiian Winter Workshop on Parameterization of Small-Scale Processes*, pp. 75–97, Hawaii Inst. of Geophys., Honolulu, 1989.

Roemmich, D., and T. McCallister, Large-scale circulation of the North Pacific Ocean, *Prog. Oceanogr., 22*, 171–204, 1989.

Roemmich, D., S. Hautala, and D. Rudnick, Northward abyssal transport through the Samoan Passage and adjacent regions, *J. Geophys. Res., 101*, 14,039–14,055, 1996.

Speer, K. G., The Stommel and Arons model and geothermal heating in the South Pacific, *Earth Planet. Sci. Lett., 95*, 359–366, 1989.

Speer, K. G., and P. A. Rona, A model of an Atlantic and Pacific hydrothermal plume, *J. Geophys. Res., 94*, 6213–6220, 1989.

Stommel, H., Is the South Pacific helium-3 plume dynamically active?, *Earth Planet. Sci. Lett., 61*, 63–67, 1982.

Stommel, H., and A. B. Arons, On the abyssal circulation of the world ocean, II, An idealized model of the circulation pattern and amplitude in oceanic basins, *Deep Sea Res., 6*, 217–233, 1960.

Taft, B. A., S. P. Hayes, G. E. Friederich, and L. A. Codispoti, Flow of abyssal water into the Samoa Passage, *Deep-Sea Res., Part A, 38*, suppl. 1, S103–S128, 1991.

Talley, L. D., Distribution and formation of North Pacific Intermediate Water, *J. Phys. Oceanogr., 23*, 517–537, 1993.

Talley, L. D., and G. C. Johnson, Deep, zonal subequatorial currents, *Science, 263*, 1125–1128, 1994.

Thompson, L., and G. C. Johnson, Abyssal currents generated by diffusion and geothermal heating over rises, *Deep Sea Res., Part I, 43*, 193–211, 1996.

Tsuchiya, M., and L. D. Talley, Water-property distributions along an eastern Pacific hydrographic section at 135°W, *J. Mar. Res., 54*, 541–564, 1996.

Warren, B. A., Transpacific hydrographic sections at Lats. 43°S and 28°S: The SCORPIO Expedition, II, Deep water, *Deep Sea Res. Oceanogr. Abstr., 20*, 9–38, 1973.

Wunsch, C., D. Hu, and B. Grant, Mass, heat salt, and nutrient fluxes in the South Pacific Ocean, *J. Phys. Oceanogr., 13*, 725–753, 1983.

G. C. Johnson, Pacific Marine Environmental Laboratory, NOAA, 7600 Sand Point Way N.E., Building 3, Seattle, WA 98115-0070. (e-mail:gjohnson@pmel.noaa.gov)

L. D. Talley, Scripps Institution of Oceanography, University of California San Diego 0230, 9500 Gilman Drive, La Jolla, CA 92093-0230. (e-mail: ltalley@ucsd.edu)

(Received October 10, 1996; revised May 13, 1997; accepted July 3, 1997.)